JOURNAL OF GEOPHYSICAL RESEARCH, VOL. 113, B04305, doi:10.1029/2007JB005180, 2008

Coseismic displacement and tectonic implication of 1951 Longitudinal Valley earthquake sequence, eastern Taiwan

Yuan-Hsi Lee,[1] Guin-Ting Chen,[1] Ruey-Juin Rau,[2] and Kuo-En Ching[2]

Received 20 May 2007; revised 21 September 2007; accepted 15 January 2008; published 17 April 2008.

[1] The Longitudinal Valley Fault (LVF) in eastern Taiwan is an extremely active fault with 3–4 cm of displacements consumed each year along its length. The fault forms the suture zone between the Philippine Sea and Eurasian plates as a result of an oblique arc continental collision. From 22 October to 5 December 1951, four earthquakes (Ms > 7) shook the LVF. We used triangulation (from 1917 to 1921 to 1976–1978) and interseismic GPS (from 1990 to 1995) data to estimate coseismic displacements of the 1951 earthquake sequences. Coseismic displacement progressively decreases from north to south and the azimuth changes from north to NE, then to a NW direction. According to the inverted faulting mechanism, the Longitudinal Valley fault can be separated into three segments. Both the northern and central segments have a high dip angle to the east, but the southern segment is of listric fault geometry. The northern segment exhibits dominantly left lateral strike-slip faulting with reverse component, while the middle exhibits thrusting dominantly, and the southern segment exhibits thrusting with left-lateral motion associated with a smaller coseismic displacement. In addition, this three-segment deformation model can explain the pattern of recent crustal deformation along the LVF and Coastal Range.

Citation: Lee, Y.-H., G.-T. Chen, R.-J. Rau, and K.-E. Ching (2008), Coseismic displacement and tectonic implication of 1951 Longitudinal Valley earthquake sequence, eastern Taiwan, *J. Geophys. Res.*, *113*, B04305, doi:10.1029/2007JB005180.

1. Introduction

[2] Taiwan orogeny results from complex tectonic interaction between the Philippine Sea plate and Eurasian plate. Northeast of Taiwan, the Philippine Sea plate is being subducted beneath the Ryukyu arc of the Chinese continental margin, while south of Taiwan island, the oceanic lithosphere of the South China Sea subducts the Philippine Sea plate. The central part represents a major collision zone between these two plates [*Biq*, 1965; *Chen and Wang*, 1986; *Ho*, 1988; *Teng*, 1990; *Malavieille et al.*, 2002] (Figure 1). The Philippine Sea plate moves in a NW direction by nearly 8 cm/a relative to the Eurasian plate, resulting in an oblique collision between the Luzon arc and the continental margin of the Eurasian plate. The Longitudinal Valley Fault (LVF) strikes NNE with high angle dip to the east. It is a suture zone that separates the Central Range (Eurasian Plate) and the Coastal Range (Philippine Sea Plate) [*Barrier and Angelier*, 1986; *Yu et al.*, 1997; *Yu and Kuo*, 2001] (Figure 1).Various types of fault creep and differing seismic rates in relation to this suture zone have been found along the LVF. For example, the relative horizontal displacement direction of GPS vectors progressively change NW to near N trending from south to north (Figure 2) [*Yu et al.*, 1997; *Yu and Kuo*, 2001]. The uplift rate is also variable along the LVF. Along the coast side of the Coastal Range, the uplift rate varies considerably. For example, north of Fengping, it is smaller than it is to the south [*Yu and Liu*, 1989; *Liu and Yu*, 1990] (Figure 3).

[3] Owing to such a high deformation rate, many earthquakes have occurred along the LVF. The 1951 earthquake sequence makes for a good example. The sequence started on Oct 25, 1951 and continued to Nov 25, 1951. It was characterized by a series of large earthquakes (4 events of magnitude greater than 7) [*Cheng et al.*, 1996] starting in the north and progressively propagating southward. Eighty-five people died and more than one thousand were hurt [*Hsu*, 1962; *Cheng et al.*, 1996; *Shyu et al.*, 2007]. Obvious surface ruptures were observed from the Hualien to Yuli areas. In some outcrops, right-lateral strike-slip faulting associated with a thrusting component were observed [*Hsu*, 1962; *Shyu et al.*, 2007].

[4] This sequence of earthquakes affords us an opportunity to interpret the characteristics of plate boundary faulting during oblique collision, but these events occurred over 50 years ago and only a little information remains. Therefore, even the source parameters of these events are widely disparate [*Taiwan Weather Bureau*, 1952; *Gutenberg and Richter*, 1954; *Lee et al.*, 1978; *Abe*, 1981; *Cheng et al.*, 1996]. Consequently, in this study, we wish to examine the coseismic displacement and faulting mechanisms of the 1951 LVF earthquake sequence using triangulation data from 1917 to 1921 to 1976–1978 in combination with

[1]Department of Earth and Environmental Sciences, National Chung-Cheng University, Chia-Yi, Taiwan.
[2]Department of Earth Sciences, National Cheng-Kung University, Chia-Yi, Taiwan.

0148-0227/08/2007JB005180$09.00

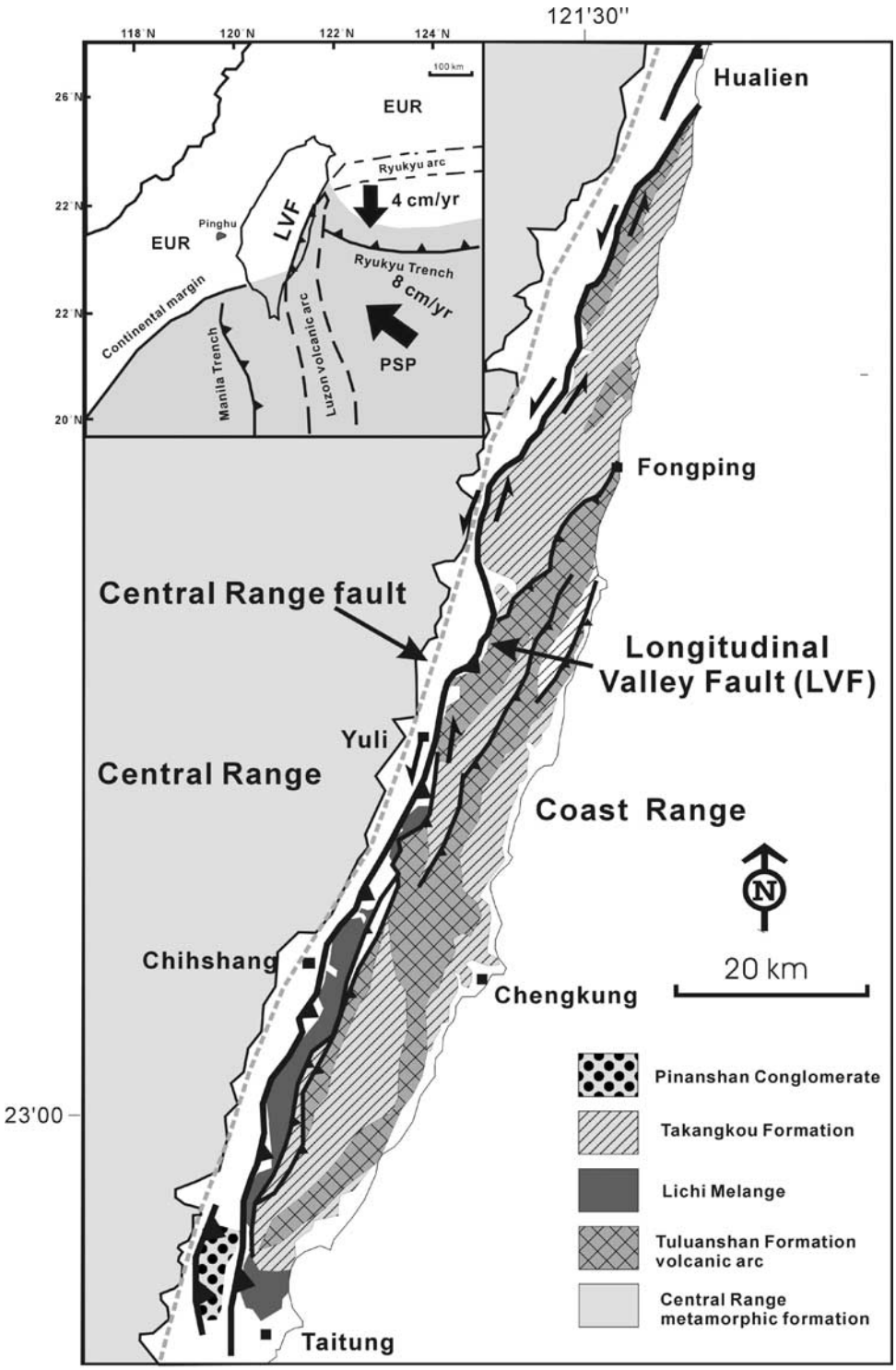

Figure 1. Schematic geological map of the Coastal Range (modified from *Chen and Wang* [1986]). Note the particular distribution of the Lichi Mélange: along the western flank of the southern Coastal Range, around the southern tip of the Coastal Range. Insert shows tectonic setting around Taiwan.

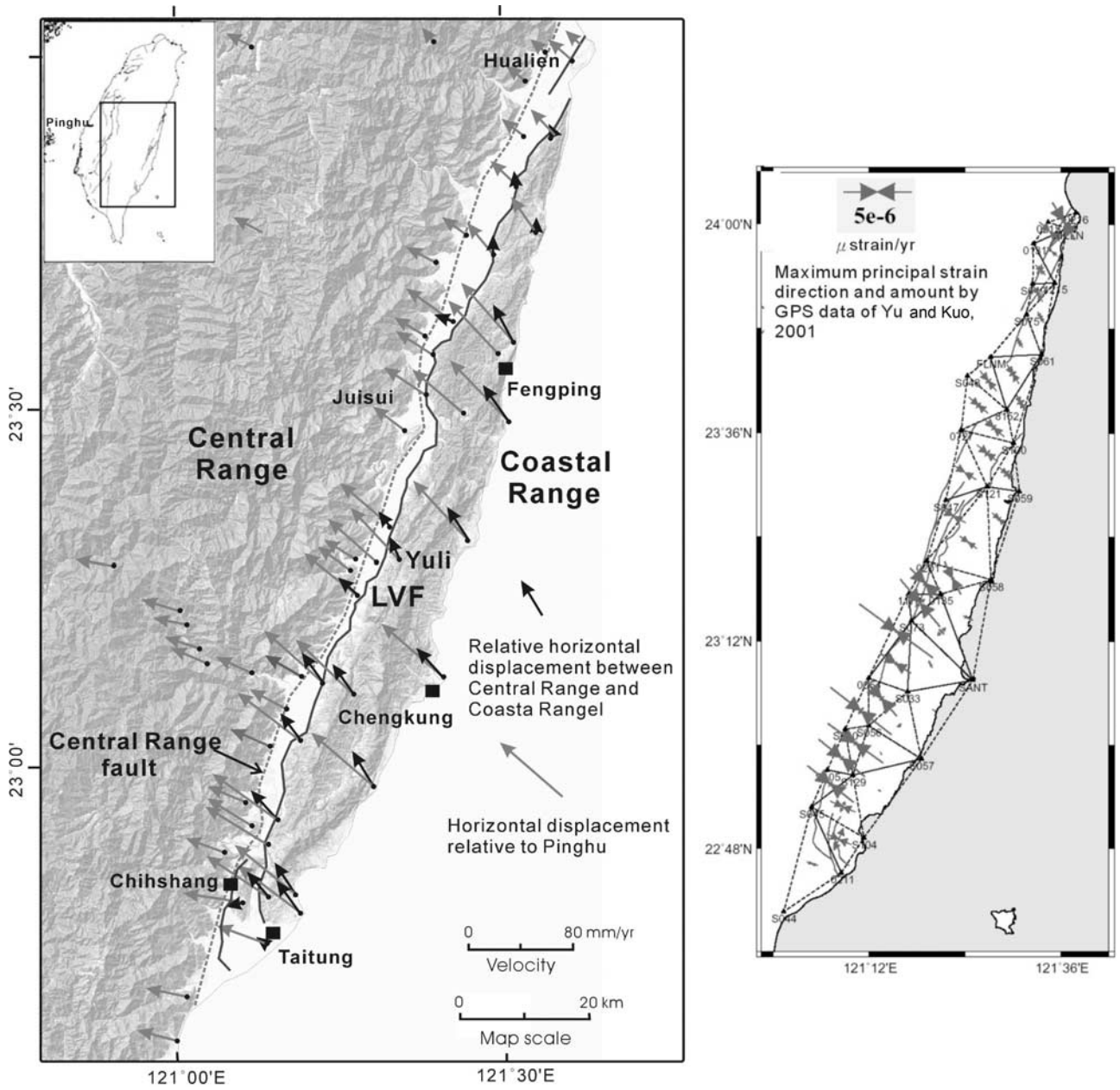

Figure 2. (left) The gray arrows are GPS velocities relative to Paisha, Penghu in the Longitudinal Valley area. The black arrows in the Coastal Range are velocities with respect to the eastern margin of the Central Range [*Yu and Kuo*, 2001]. (right) We calculated the principal strain direction and magnitude by GPS velocity of *Yu and Kuo* [2001]. The azimuth of principal strain direction rotates clockwise from south to north of the Coastal Range.

interseismic GPS displacement data from 1990 to 1995 [*Lee and Yu*, 1987; *Yu et al.*,1997]. We believe such an examination would be invaluable in helping to explain the variable crustal deformation pattern along the LVF and Coastal Range.

2. Geological Background of the Longitudinal Valley Fault (LVF)

[5] The Longitudinal Valley of eastern Taiwan at 150 km long and NNE-striking is a suture zone between the Eurasian plate and Philippine Sea plate [*Biq*, 1965; *Ho*, 1988; *Teng*, 1990] (Figure 1). On its eastern side is the Coastal Range, an assemblage of Miocene through early Pliocene units of the Luzon island arc and a highly deformed forearc basin system which is composed of turbidite deposits, mélange and fringing-reef limestone. In the southwestern flank of the Coastal Range, the Lichi Formation is a distinct unit composed of chaotic mudstones intermixed with exotic blocks of various size and lithology. The chaotic clayey mudstone associated with intense scaly foliation of the Lichi Formation [*Hsu*, 1956] was first recognized as a mélange by *Biq* [1965]. Although the LVF has a similar tectonic setting, the Lichi mélange only occurs in the southern part of the

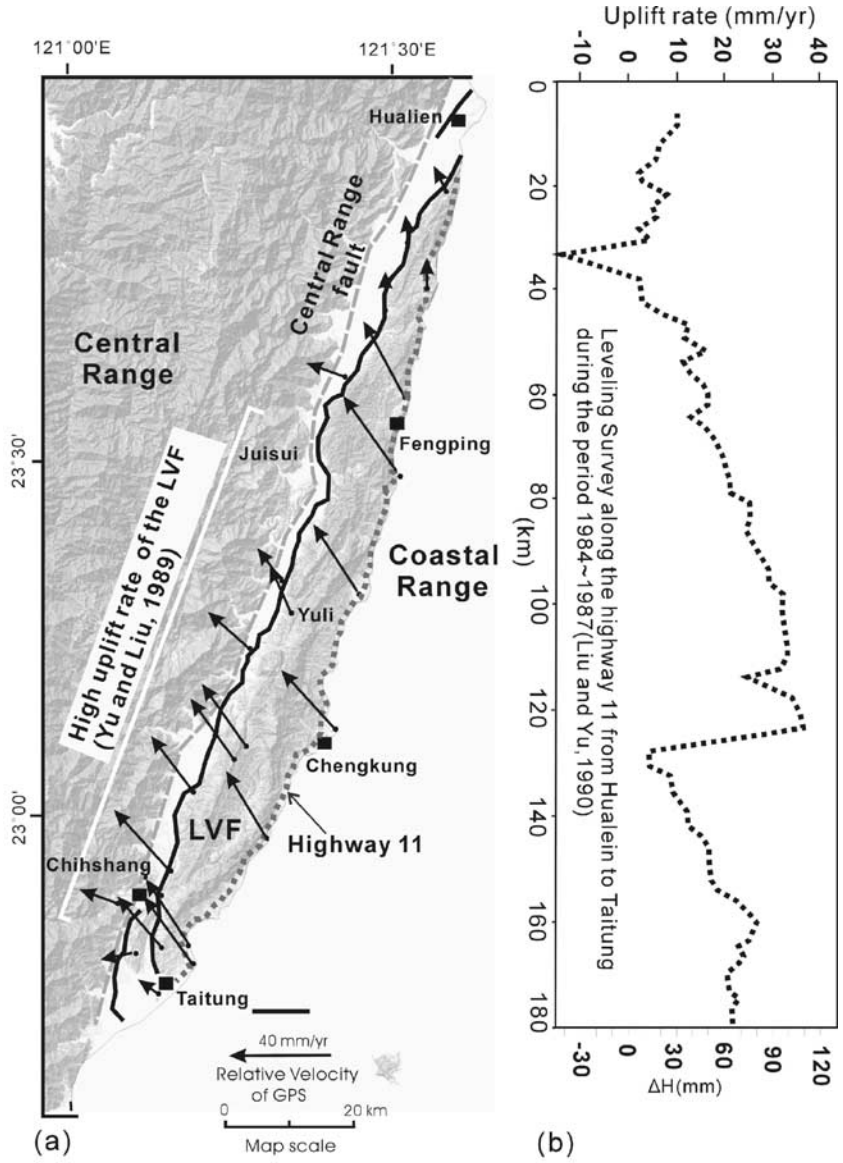

Figure 3. Recent crustal deformations around the Coastal Range and the LVF. (a) From Juisui to Chihshang the LVF shows a high uplift rate according to a short leveling survey [*Yu and Liu*, 1989]. The black arrows in the Coastal Range are velocities with respect to the eastern margin of the Central Range. (b) Along Highway 11 in the eastern side of the Coastal Range, the uplift rate progressively increases from north to south and then suddenly drops around Chengkung and then increases again [*Liu and Yu*, 1990].

LVF. On the western side of the Longitudinal Valley is the eastern flank of the Central Range, which is composed of Mesozoic to Paleogene metamorphic rocks (Figure 1) [*Barrier and Angelier*, 1986; *Chen and Wang*, 1986; *Ho*, 1988; *Chang et al.*, 2001].

[6] In this suture zone, two major faults have been identified by previous studies. One is the Central Range fault and the other is the Longitudinal Valley Fault (LVF). Although both faults are active, recent GPS data indicates the Central Range fault to be relatively stable when compared with the LVF, which is very active with 3∼4 cm/a of displacements being consumed along its length, resulting in high seismicity [*Yu et al.*, 1997; *Yu and Kuo*, 2001; *Kuochen et al.*, 2004; *Shyu et al.*, 2006] (Figures 1 and 2). According to geomorphic evidence, the northern part of LVF is left-lateral strike-slip faulting dominantly, and from the central to southern part of the LVF there is thrusting associated with a left-lateral component [*Shyu et al.*, 2005, 2007].

3. Crustal Deformation Around the LVF

[7] The Longitudinal Valley in eastern Taiwan is one of the best-instrumented deformation zones in the world. Different types of studies utilizing seismic, GPS, trilateration, creepmeters, and geomorphic methods have been conducted in the region. These types of studies have recorded complex and laterally variable slip behavior along the fault.

[8] Using the trilateration network, *Yu et al.* [1990] calculated relative displacement between the Central Range and Coastal Range. Their study gave relative displacement to be 34 mm/a in a direction of 314° for the southern segment; however, toward the northern segment relative displacement progressively declined to be 25 mm/a in a N-S direction [*Yu*, 1989; *Yu and Liu*, 1989; *Yu et al.*, 1990] (Figure 2). A short leveling survey across the LVF showed a high uplift rate in the central segment of the LVF, extending from Juisui to Chihshang [*Yu and Liu*, 1989; *Liu and Yu*, 1990; *Yu et al.*, 1990] (Figure 3a). Another leveling survey along Highway 11 of the coastal side of the Coastal Range shows that the uplift rate is relatively small to the north of Fengping, while toward the south it increases progressively. Around the Chengkung area, the uplift rate dramatically decreases, and then becomes progressively larger again. The highest uplift rate reaches 30 mm/a (Figure 3b) [*Liu and Yu*, 1990]. *Liu and Yu* [1990] considered compressional tectonic force not applying in the northern part of the Coastal Range, resulting in lower vertical displacement and multiple breakages of the plate along the coast. This, they conclude, may be the most important factor for the complexity of vertical displacement [*Liu and Yu*, 1990].

[9] In order to clarify the structural style of the LVF, *Yu and Kuo* [2001] fixed GPS stations on the Central Range, which borders the LVF, to show the relative displacements between the Coastal Range and Central Range. They also found that the Coastal Range systematically changes movement direction from northwestward to northward from south to north. The relative crustal motions are 15–15.2 mm/a at 330–0° in the northern segment of the LVF. In the central segment the relative crustal motions are 13.3–24.9 mm/a at 309–336°. In the southern, segment the relative crustal motions are 29.2–32.7 mm/a at 312–323° [*Yu and Kuo*, 2001] (Figure 2). We calculated maximum principal strain direction using the GPS data of *Yu and Kuo* [2001], which also showed progressive clockwise rotation from 308° in the south to 330° in the north (Figure 2).

[10] Figure 4 shows 3D relocated seismicity around the LVF. In the northern part many earthquakes have occurred in both the Central and Coastal Ranges; however, in the central part only a few earthquakes have occurred. According to seismicity data, the LVF seems to exhibit high angle dip from the northern to central parts. The southern part of the LVF shows listric fault geometry. A recent destructive earthquake along the southern LVF occurred in 2003, the Chishang earthquake (Mw 6.8) [*Wu et al.*, 2006; *Hu et al.*, 2007; *Ching et al.*, 2007].

[11] Although a lot of research has been conducted on the deformation rate of the LVF, most of the results relate to recent crustal deformation and there has been no research discussing the deformation mechanism of the 1951 LVF sequence. The main reason being that there is little information relating to this earthquake sequence. The only relevant data was obtained by *Lee and Yu* [1987], who calculated relative displacement between the Coastal Range and Central range by utilizing the 1st to 3rd classes of the triangulation network from 1917 to 1921 to 1976–1978. They found that the displacement amounts ranged from 2.5∼4.4 m, which were larger than the interseismic displacement amount over sixty years. *Lee and Yu* [1987] concluded that these displacements include the interseismic displacement and coseismic displacement of the 1951 earthquake.

4. Characteristics of the 1951 LVF Earthquake Sequences

4.1. Coseismic Displacement of the 1951 Earthquake Sequences

[12] In eastern Taiwan 1st to 3rd class triangulation point surveys were conducted separately during 1917–1921 and 1976–1978. Both surveys were based on different geodetic reference systems, the Hayford and Kaula systems, which means that we cannot compare them directly to obtain displacement. Because of the original data being unavailable, *Lee and Yu* [1987] used Cunningham's azimuth formula [*Bomford*, 1980] to invert triangulation point coordinates back to the original horizontal angle observation for both surveys. H1 and H2 are the horizontal angle of first and second time measurements for the different coordinate systems. They used network adjustment with minimum constraints and similarity transformation to recalculate H1 with the Kaula geodetic reference system and compared these results with the results of H2 to obtain the relative displacement [*Lee and Yu*, 1987].

[13] These displacement vectors are possibly the only data relating to the 1951 earthquake sequence available. They combine interseismic displacement over the 60 year window and coseismic displacement for the 1951 sequence. One method of obtaining the coseismic displacement of the 1951 earthquakes is to subtract interseismic displacement. The displacement vectors of the first- to third-order triangulation data are fixed to different control points. In order to calculate, coseismic displacement, we recalculated all the data to be fixed at one control point, T10 (Figure 5). Second, we assumed that GPS data collected from 1990 to 1995 can stand as proxy data for the long-term interseismic displacement rate over sixty years (Figure 2) [*Yu et al.*, 1997]. Then we recalculated the GPS data to be fixed at T10. Third, because the control points of the triangulation network and GPS are not at the same position, we interpolated the GPS data to the triangulation network control points to obtain the interseismic displacement rate on the triangulation network control points. Then, we extrapolated the interseismic displacement rate of the triangulation network control points to sixty years (Figure 6). Fourth, we obtained the coseismic displacement of the 1951 earthquake sequence by subtracting the interseismic displacement amount of sixty years from the displacement vectors of the triangulation network control points (Figure 7). Here we inverted the first- to third-order triangulation network data on the Coastal Range and the first-order triangulation data on the western side of the Coastal Range for the coseismic slip distribution on the fault plane. The reason why we only used the first-order triangulation data on the western side of the Coastal Range is that the data quality of these first-order triangulation stations, located in the mountain area, is better. The coseismic displacement vectors of the 1951 Longitudinal Valley earthquake sequence are shown in Table 1 and Figure 7. The horizontal displacement magnitude progressively decreases from north to south and the azimuth of displacement vectors change from north-trending in the

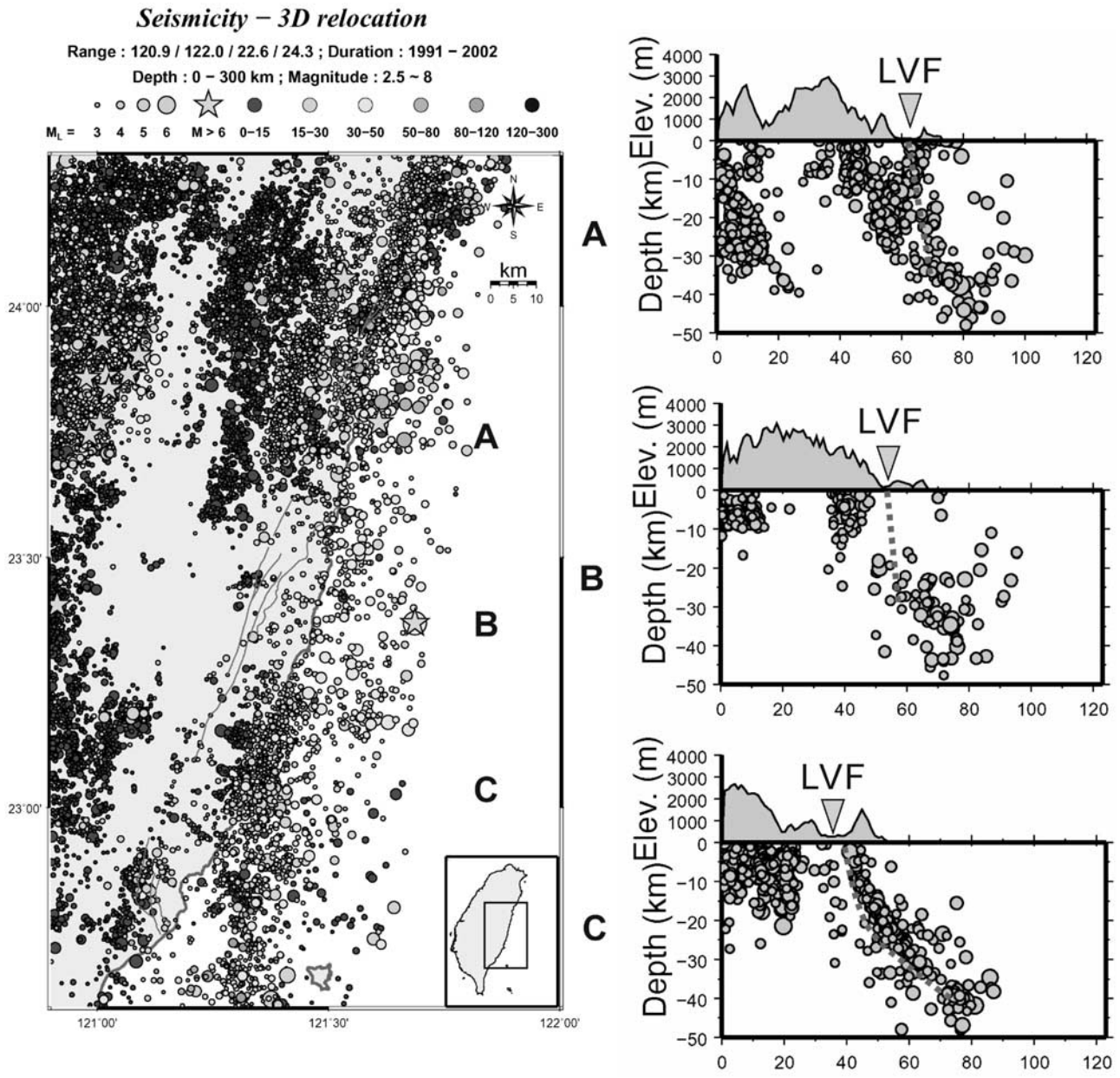

Figure 4. (left) The 3-D relocation seismicity around the LVF. (right) The seismicity profile across northern, central, and southern segments of the LVF. The red dotted lines indicate the possible fault plane. These three profiles show different earthquake distribution. The fault plane seems high angle dipping to the east in profiles A and B, and profile C shows listric fault geometry.

northern segment to NE-trending in the central segment, and finally, NW-trending in the southern segment.

4.2. Dislocation Model of the 1951 Earthquake Sequence

[14] According to the spatial distribution feature of coseismic displacements, we consider the entire LVF as being active during the 1951 earthquake sequence. To estimate the coseismic slip distribution on a given fault plane, we inverted our horizontal coseismic offsets by using the Poly3Dinv code [*Maerten et al.*, 2005]. This approach is developed on the basis of a solution of an angular three dimensional dislocation in a linear, homogeneous, and isotropic elastic half space. Unfortunately, the fault geometry parameters such as fault width and dip angle are not clear for the 1951 earthquake. Therefore we used the genetic algorithm (GA) method to search the optimal dip angle and fault width of the LVF. The GA works on a set of models (chromosomes) called a population at the same time. Each model consists of a parameter set like genes in a chromosome. The population of individuals is initially randomly created and evolves by natural selection through three operations: reproduction, crossover, and mutation. For the GA method, we used the program proposed by D.L. Carroll's FORTRAN Genetic Algorithm Driver (1999, version 1.7a; download from http://cuaerospace.com/carroll/ga.html). The same probability of crossover is given to each bit of

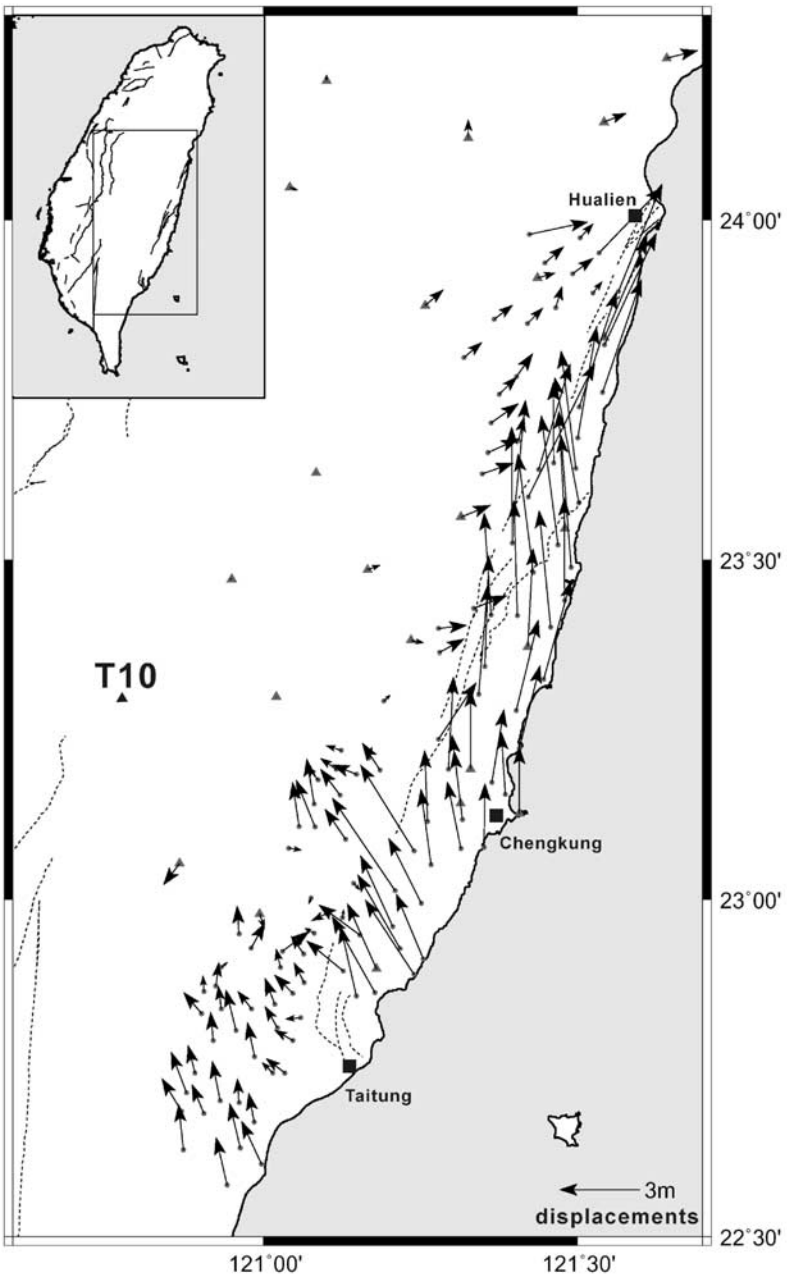

Figure 5. Relative displacement between the Coastal Range and Central Range according first and third classes of the triangulation network from 1917 to 1921 to 1976–1978. These displacements include interseismic displacements over approximately 60 years and coseismic displacement of the 1951 LVF earthquake sequences. Those displacement vectors are fixed to T10 [*Lee and Yu*, 1987].The triangles and circles are first and second to third class of the triangulation network stations.

the chromosome and the probability is equal to 0.5. Mutations occurred with the probability 0.04. The fitting index F (misfit) is the sum of the absolute differences between calculated and measured displacements in two components as defined by equation (1),

$$F = \sqrt{\frac{\sum_{i=1}^{k} \left(C_i\left(d_i^{cal} - d_i^{obs}\right)\right)^2}{\sum_{i=1}^{k} C_i}}, \qquad (1)$$

where k is the number of observations of the two displacement components; d_i^{cal} is the ith calculated displacements, which are evaluated by Poly3D software [*Thomas*, 1993]; d_i^{obs} is the ith observed displacements; and C_i is the ith weighting, which is defined by $1/\sigma_i$. To minimize this fitting index is the goal of evolution.

[15] First we assumed the rupture segment of the LVF as being a single fault plane and we used the GA method to search the best fit fault geometry. The resultant comparison between observations and synthetics of this model is good enough for the northern segment of the study area. In

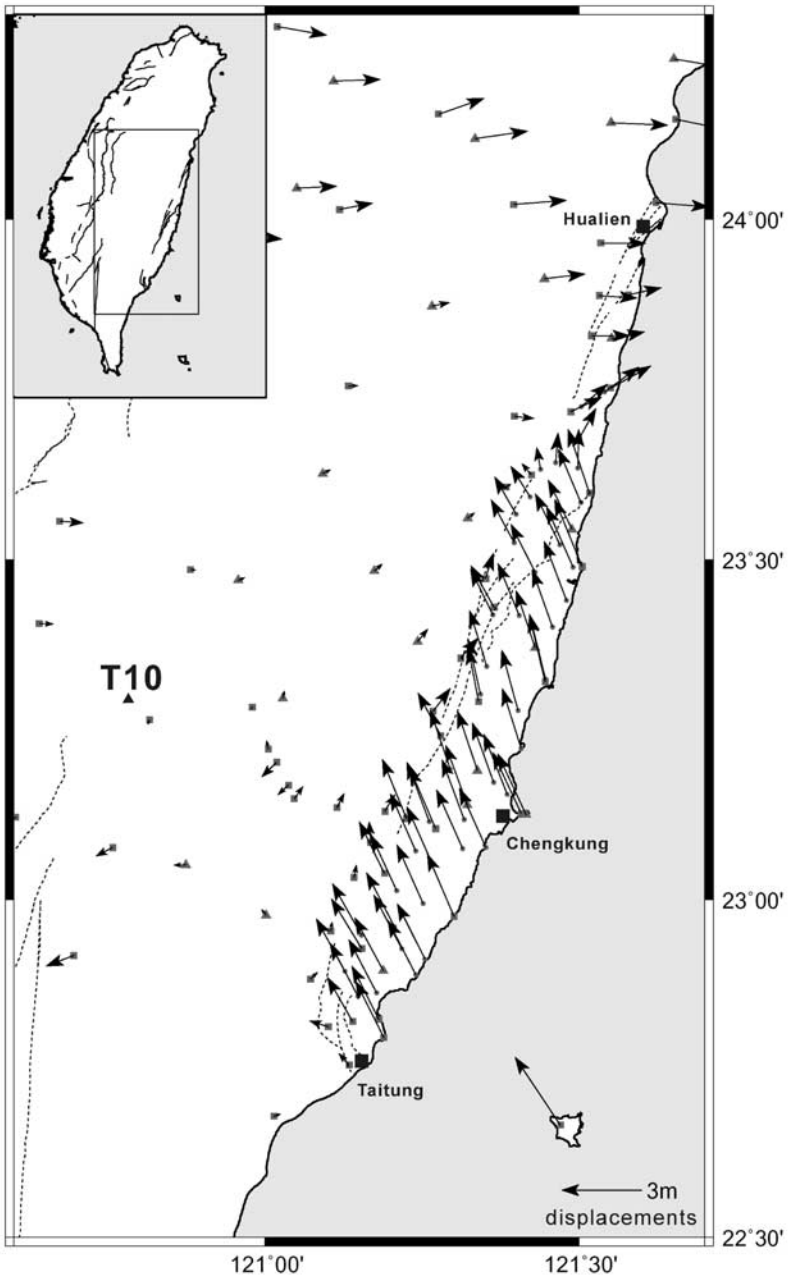

Figure 6. Sixty-year interseismic displacements of the GPS stations and triangular control points relative to T10. The displacements of triangular control points were calculated by interpolating the GPS data to the triangulation network control points. The rectangles are GPS control points and the triangles and circles are first- to third-class triangular control points.

contrast, the comparison shows a larger misfit in the southern part. To improve the modeling results in the southern part of the network, we adopted the listric fault geometry of the Chihshang fault, given by *Hu et al.* [2007] as the southern segment geometry of the LVF. These fault geometry parameters are inferred by fitting the shape of the aftershock distribution associated with the 2003 Mw 6.8 Chengkung, Taiwan earthquake in SE Taiwan [*Hu et al.*, 2007]. For the northern segment of the LVF from Hualien to Yuli, we used the GA method to find the optimized fault geometry parameters. The optimal dip angle of the LVF from Hualien to Yuli is ca. 67° dipping to the east and its fault width is ca. 35 km. In this study the optimal smoothing parameter is selected on the basis of searching the inflection point of the trade-off curve of the average RMS square misfit and the model roughness, where the model roughness is defined as the reciprocal of smoothing parameter. Hence the smoothing parameter of 1.5 is adopted for this best fit model with the data misfit as 42.77 cm (Figure 8). The observed and modeled displacement vectors have good correlation (Figure 9b). The inverted slip amount progressively decreases from north to south along the LVF (Figure 9a). The northern segment dominantly acts as strike-slip faulting with reverse component in the northernmost part. The

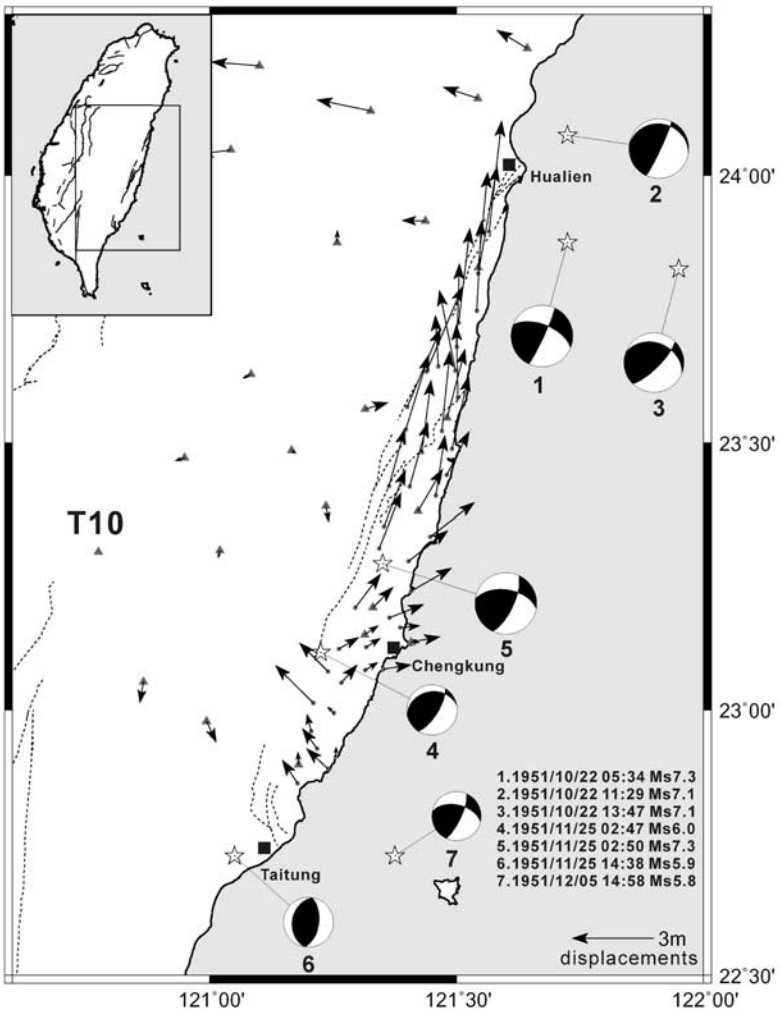

Figure 7. Coseismic displacement of the 1951 LVF earthquake sequence. The vectors show the coseismic displacements of the 1951 LVF earthquake sequence, which is relative to the T10 control point. The focal mechanism of the 1951 LVF is based on work by *Cheng et al.* [1996].

central segment is thrusting in the deeper part and left-lateral strike-slip component in the shallow part. For the southern segment of the LVF, the Chihshang fault, the oblique slips prevail along the fault plane with rather small slip values (Figure 9a). In addition, we inferred vertical coseismic ground displacements on the basis of forwarding the derived coseismic slip distribution (Figure 9c). The resultant displacement field shows that the magnitudes of vertical displacements are quite small at the northern segment of the Longitudinal Valley. On the contrary, south of the Fengping area the magnitudes of vertical displacements progressively increase southward (Figure 9c). The total geodetic magnitude associated with this event derived from the inverted fault slip is Mw 7.7, which is similar to the observed magnitude (Ms = 7.3, 6.0, and 7.3). Besides, the estimated average rake angle is also comparable to the result of the fault plane solution of the 1951 earthquake sequence by *Cheng et al.* [1996].

4.3. Segmentation of the 1951 Longitudinal Valley Fault

[16] The largest horizontal displacement is about 4 m in the north of the LVF and progressively decreases to the south. The displacement azimuth is in a northward direction in the northern part and changes to a NE direction in the central part and then to a NW direction in the south. This displacement amount and azimuth suggest that LVF has different faulting mechanisms. Our inverted results show there are different faulting parameters from north to south; therefore, we suggest that the LVF can be separated into three segments (Figure 9a). Both northern and central segments are high angle dipping to the east but the southern segment is of listric fault geometry. The northern segment is dominantly left lateral strike-slip faulting with thrust component in the northern most part and the central segment exhibits thrusting dominantly with strike-slip component in the upper part. The southern segment of the LVF exhibits thrusting with a left-lateral component associated with smaller displacement on this listric fault.

[17] The interseismic earthquake distribution also supports that there are three segments along the LVF. According to the earthquake distribution, the northern segment experienced many earthquakes around the LVF while the central segment earthquakes only occurred at depths of more than 20 km. The southern segment earthquake distri-

Table 1. East and North Components, Coseismic Horizontal Displacement, and Azimuth of Coseismic Horizontal Displacement[a]

Trilateration Control Point	Longitude	Latitude	E, cm	N, cm	S, cm	Azi, deg
t01	121.544	23.827	34.8	351.7	353.4	5.6
t02	121.481	23.547	66.4	254.3	262.8	14.6
t03	121.422	23.372	91.0	155.2	179.9	30.4
t04	121.330	23.192	74.8	76.3	106.9	44.4
t05	121.314	23.142	50.0	33.1	59.9	56.5
t06	121.408	23.127	106.7	20.4	108.7	79.1
t07	121.180	22.897	−2.6	47.7	47.8	356.9
t08	120.994	22.979	35.8	−78.4	86.2	155.4
t09	120.866	23.053	−13.8	−78.8	80.0	190.0
t10	120.774	23.296	0.0	0.0	0.0	0.0
t11	121.021	23.299	−6.4	−28.0	28.7	192.9
t12	121.235	23.382	10.8	−56.8	57.8	169.3
t13	120.949	23.472	−34.7	−10.7	36.3	252.8
t14	121.315	23.563	85.5	24.7	89.0	73.9
t15	121.166	23.486	16.2	−10.4	19.3	122.7
t16	121.084	23.629	−30.3	−15.5	34.0	242.9
t17	120.973	23.747	−2.1	−4.2	4.7	206.3
t18	121.258	23.875	1.0	45.2	45.2	1.2
t19	121.437	23.915	−85.9	1.5	85.9	269.0
t20	121.042	24.048	−121.5	−16.3	122.6	262.4
t21	121.326	24.120	−198.7	41.3	202.9	258.3
t22	121.101	24.205	−175.9	14.2	176.4	265.4
t23	121.543	24.144	−128.4	41.5	134.9	287.9
t24	121.643	24.237	−112.0	67.2	130.6	301.0
t25	121.224	24.385	−202.5	9.6	202.7	272.7
t26	121.431	24.364	−198.9	102.4	223.7	297.2
t27	121.683	24.393	−163.5	69.0	177.5	292.9
t28	121.556	24.511	−198.4	38.5	202.1	281.0
a02	121.566	23.895	46.2	407.5	410.1	6.5
a03	121.544	23.817	69.4	394.1	400.2	10.0
a04	121.541	23.747	17.3	331.1	331.6	3.0
a05	121.504	23.725	41.7	347.9	350.4	6.8
a06	121.501	23.680	9.4	306.7	306.9	1.8
a07	121.498	23.635	−59.0	295.0	300.8	348.7
a08	121.503	23.584	−5.8	269.5	269.5	358.8
a09	121.463	23.643	−11.1	188.7	189.1	356.6
a10	121.439	23.633	133.0	313.7	340.7	23.0
a13	121.470	23.522	29.7	294.3	295.8	5.8
a14	121.491	23.489	61.5	269.3	276.2	12.9
a15	121.480	23.440	82.9	161.2	181.3	27.2
a16	121.400	23.567	122.7	287.7	312.8	23.1
a18	121.397	23.525	84.3	275.1	287.8	17.0
a19	121.430	23.482	33.8	265.6	267.7	7.2
a21	121.405	23.418	67.0	236.6	245.9	15.8
a22	121.363	23.419	58.2	211.3	219.1	15.4
a23	121.458	23.401	33.3	222.0	224.5	8.5
a24	121.353	23.344	78.8	207.0	221.5	20.8
a25	121.343	23.303	80.4	204.2	219.5	21.5
a26	121.447	23.325	163.2	125.1	205.6	52.5
a27	121.403	23.279	144.5	112.8	183.3	52.0
b01	121.295	23.192	93.5	124.6	155.7	36.9
b03	121.364	23.173	126.4	49.1	135.6	68.8
b04	121.408	23.223	148.9	85.8	171.8	60.0
b05	121.386	23.155	73.0	6.9	73.3	84.6
b06	121.262	23.115	73.6	42.8	85.2	59.8
b07	121.317	23.118	51.9	32.7	61.3	57.8
b08	121.267	23.051	58.6	66.5	88.6	41.4
b09	121.315	23.075	47.4	29.1	55.6	58.5
b10	121.352	23.077	103.1	16.3	104.4	81.0
b11	121.240	23.072	−104.6	105.6	148.7	315.3
b12	121.210	23.013	−139.4	138.3	196.3	314.8
b13	121.252	22.994	−24.3	23.6	33.9	314.3
b14	121.206	22.960	−16.3	62.9	65.0	345.5
b15	121.218	22.927	−54.1	74.2	91.8	323.9
b16	121.255	22.912	2.0	36.3	36.4	3.1
b18	121.240	22.889	−78.6	74.9	108.6	313.6
b21	121.178	22.862	−56.4	86.0	102.9	326.7

[a]E, east component; N, north component; S, coseismic horizontal displacement; Azi, azimuth of S.

bution shows a listric fault geometry (Figure 4). This difference in earthquake distribution along the LVF indicates the possibility of different faulting mechanisms.

[18] Why does the LVF have different characteristics from south to north? We speculate that this could be the result of variation in the tectonic setting from south to north (Figure 1). The Philippine Sea plate subducts the Eurasia Plate with northward motion around the northeast of Taiwan, which could result in the northern segment of the LVF having more northward motion associated with left-lateral strike slip faulting dominantly. The central segment is located in the major collision zone. The relative crustal motion direction between the Coastal Range and Central Range is NW trending resulting in dominantly thrusting. The southern segment is located at the boundary between the collision and subduction zone, resulting in listric fault geometry which is different to the central segment that exhibits a high-angle-dipping fault plane.

4.4. Comparison With Surface Deformation and Seismological Data

[19] Geomorphic evidence shows the northern segment is strike-slip faulting dominantly and the central to southern segment is thrusting with a left-lateral component that is consistent with our inverted results [*Shyu et al.*, 2005, 2007]. According to some outcrop observations of the 1951 earthquake sequence, the northern part of the LVF exhibits relatively large left-lateral strike slip motion, the middle part thrusting dominantly with left-lateral motion, and the southern part smaller displacement [*Hsu*, 1962; *Shyu et al.*, 2007]. This pattern is similar to our calculated coseismic displacement and results of the inverted faulting mechanism and can be identified in our calculations. Recently, *Cheng et al.* [1996] used S-P times, a Monte Carlo algorithm, and maximum ground motion amplitudes to

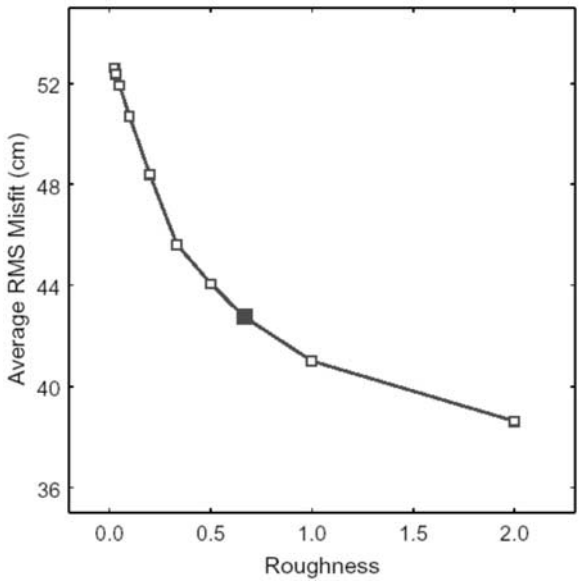

Figure 8. Trade-off curve with the average RMS square misfit function plotted as a function of the model roughness. The misfit improves with increasing model roughness. The selected roughness value is decided by the inflection point (black square) of the trade-off curve.

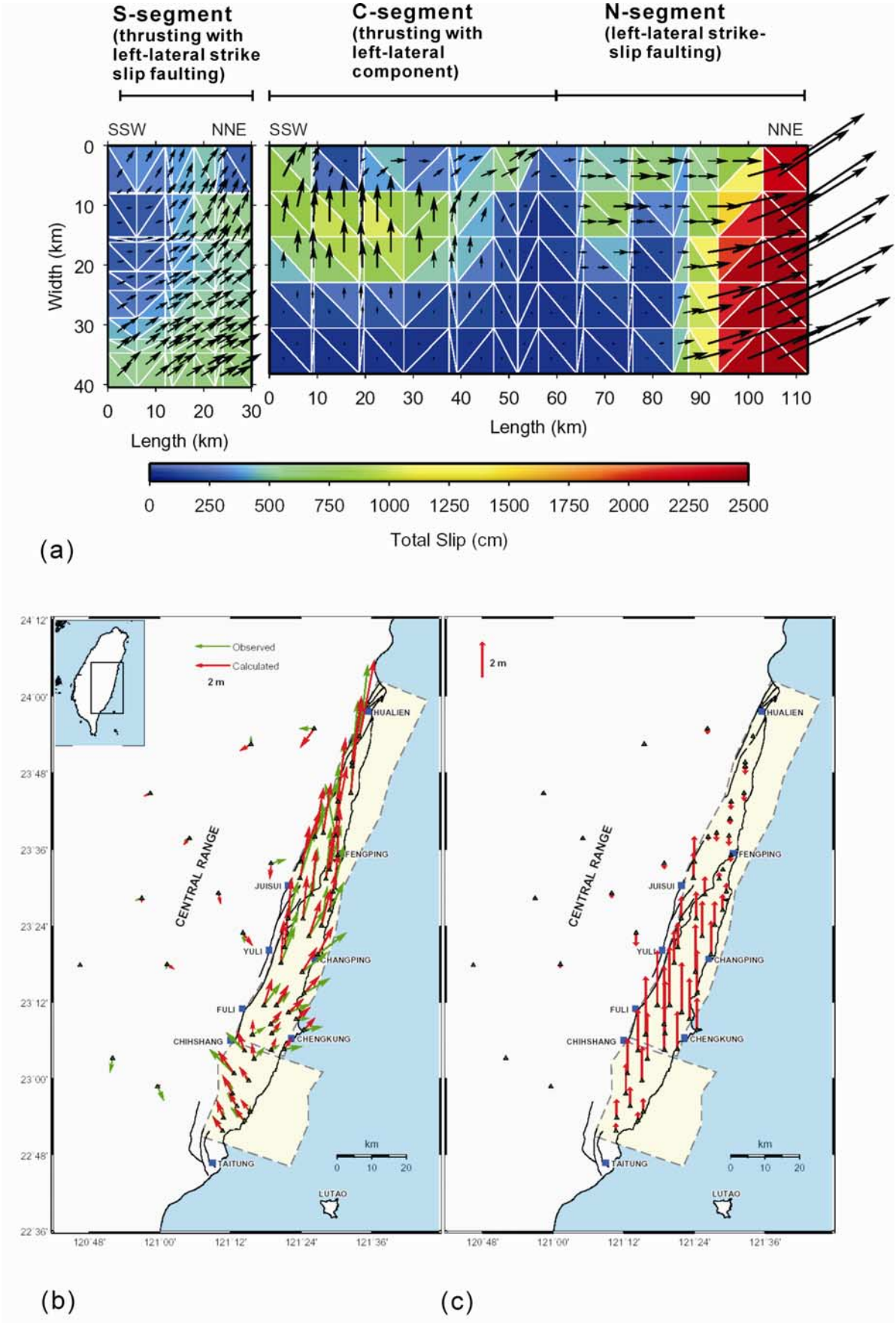
S-segment
(thrusting with left-lateral strike slip faulting)
C-segment
(thrusting with left-lateral component)
N-segment
(left-lateral strike-slip faulting)
SSW
NNE
SSW
NNE
Width (km)
Length (km)
Length (km)
Total Slip (cm)
(a)
Observed
Calculated
2 m
HUALIEN
FENGPING
JUISUI
YULI
CHANGPING
FULI
CHIHSHANG
CHENGKUNG
TAITUNG
LUTAO
CENTRAL RANGE
km
(b)
(c)

Figure 9

relocate the epicenters and calculate the magnitudes and focal mechanism for these events. There were 4 earthquakes of magnitude larger than 7. Figure 7 shows the faulting mechanism of major events during the 1951 earthquake sequences. Events 1, 4, and 5 are major events associated surface rupture. The events represent cases of dominantly strike-slip faulting, dominantly thrust faulting with a strike-slip component, and dominantly thrust faulting, respectively. According to Cheng's results, the first earthquake (1951/10/22 05:34 Ms 7.3) is dominantly strike-slip faulting, which is similar to our inverted result [*Cheng et al.*, 1996] (Figures 7 and 8). This event is closer to the northern part of the LVF and we consider the surface deformation of the northern segment to be the result of this event. The fifth event (1951/11/25/02:50 Ms 7.3) is thrust faulting with strike-slip component. This is also similar to our result. The fourth event (1951/11/25 02:47 Ms 6.0) is probably associated with the southern part of the LVF. This event is dominantly thrust faulting with a smaller displacement. This result is also similar to our own. From the northern to central segment of the LVF, our inverted fault plane is ca. 67° dipping to the east, which is similar to the interseismic seismic and geological data (Figure 4).

5. Mechanism for Recent Crustal Deformation Along the LVF and Coastal Range

[20] Our inverted model shows that the lateral variations in slip behavior could explain the recent crustal deformation pattern revealed by GPS and leveling data (Figures 2 and 3). *Yu and Kuo* [2001] considered the possible existence of several NE-striking thrusts in a horsetail pattern in the northern Coastal Range to explain the near north-trending relative horizontal displacement between the Central Range and Coastal Range. *Liu and Yu* [1990] considered compressional tectonic forces not applying in the northern part of Coastal Range, resulting in lower vertical displacement and the multiple breakages of the plate that exist along the coast. Our forward vertical displacement pattern shows small subsidence in the northern segment and high vertical displacement in the central segment that progressively decreases toward the southern segment (Figure 9c). The interseismic uplift rate shows to be relatively small in the northern part of the LVF and Coast Range and progressively increases to the south. Our inverted vertical displacement pattern is similar to the recent uplift rate indicating that they could have a similar deformation mechanism.

[21] Why is relative crustal motion near N trending to the north of Fengping (Figures 2 and 3)? This can also be explained by the northern segment of the LVF being dominantly left-lateral strike slip faulting resulting in crustal motion being north trending with low vertical displacement as strain energy accumulates. In addition, we have determined the reason for the uplift rate to suddenly drop around the Chengkung area and increase again toward to the south (Figure 3). This is because the Chengkung area is near the boundary between the central to southern segment where the uplift rate drops suddenly; however, the character of the southern segment being predominantly thrusting results in the uplift rate increasing again. In the southern segment, the vertical displacement and relative displacement is high between the Coastal Range and Central Range, but it had the smallest coseismic displacement during the 1951 earthquake sequence. The southern segment of the LVF, Chihshang fault, was active again in 2003 indicating that the southern segment has the shortest earthquake interval of these segments. Although the interseismic strain rate is nearly the same between the southern and central segment the short earthquake interval in the southern segment results in less strain energy being released in each event. That is why the southern segment had the smallest coseismic displacement of the 1951 earthquake sequence. Comparing the central and southern segment of the LVF, both faults have a similar interseismic creep rate [*Yu et al.*, 1997; *Yu and Kuo*, 2001]; however, in this case, why then is the recurrence interval of Chishang fault shorter than other segments? Although the fault geometry of Chishang fault is different from the other segments, the fault geometry cannot be the reason for a shorter recurrence interval. A shorter recurrence interval could indicate friction on the fault plane could be so low that it results in lower strength of the fault zone. Comparing the faulted rock along the LVF, only the southern segment is composed of thick mudstones with scaly foliation, the Lichi Formation; and this could be the major cause for the low-friction fault zone (Figure 1). Another mechanism might be that there are fairly small asperities in the southern segment of the LVF that build up stress faster than larger asperities in the central to northern segments of the LVF.

6. Possible Errors in Coseismic Displacement

[22] There are some assumptions that could result in errors. First, we assume that the interseismic displacement rate is the same over sixty years and this may cause some errors. As the displacement pattern of the GPS is quite stable, we consider this error to be small. We interpolate the GPS data to the triangulation network control points to obtain the interseismic displacement rate of the triangulation network control points that also could results in some errors. The triangulation survey data were measured 90 and 30 years ago giving some errors that were hard to control.

[23] Considering all these conditions, we think possible errors could be less than 1 m and are more likely about 0.5 m. Although the existence of errors is hard to control, our inverted results show similar deformation mechanisms with seismological results and surface rupturing of the 1951 earthquake sequence. We consider the errors are likely to result in different displacement amounts on the fault plane

Figure 9. Maps showing the inverted and observed displacements from the triangulation network, for both (a) slip vectors on the fault plane (northern segment is left lateral strike-slip faulting and the central to southern segments are thrusting with left lateral components) and (b) the predicted and observation horizontal displacement. The yellow squares are the projections of the modeled fault planes (see details in text). Green arrows are observed data and red arrows are modeled data. (c) Predicted vertical displacement.

but that the overall displacement patterns and deformation mechanisms will be similar.

7. Conclusion

[24] 1. We used triangulation data from 1917 to 1921 to 1976–1978 in combination with interseismic displacement data from 1990 to 1995 to obtain the coseismic displacement of the 1951 LVF earthquake sequence. The coseismic horizontal displacement is about 4 m in the north and progressively decreases to the south. The displacement azimuth is to the north in the northern part, in a NE direction in the central part and then changes to a NW direction in the south. The predicted vertical displacement shows a lower vertical displacement in the northern segment, and then progressively increases in the central segment, before finally decreasing in the southern segment.

[25] 2. According to coseismic displacement and the inverted faulting mechanism, the LVF can be separated into three segments. The fault geometry of the northern and central segments exhibits a high dipping angle to the east and the southern segment is of listric fault geometry. The northern segment is strike-slip faulting dominantly with thrust component; the central segment exhibits thrusting dominantly with a left-lateral component. The southern segment exhibits thrusting with a left-lateral slip motion of smaller slip on listric fault geometry. This three segment faulting model not only shows the various faulting parameters of the 1951 earthquake sequence but also can explain the recent crustal deformation along the LVF and Coastal Range.

[26] **Acknowledgments.** We are grateful to Roland Burgmann and one anonymous reviewer for constructive and helpful reviews of the manuscript. This project was supported by the National Science Council, Taiwan, under grant NSC 94–2119-M-194–001. The GMT software of *Wessel and Smith* [1995] was used in constructing most of the figures.

References

Abe, K. (1981), Magnitudes of large shallow earthquakes from 1904 to 1980, *Phys. Earth Planet. Inter.*, *27*, 72–92, doi:10.1016/0031-9201(81)90088-1.

Barrier, E., and J. Angelier (1986), Active collision in eastern Taiwan: The Coastal Range, *Tectonophysics*, *125*, 39–72, doi:10.1016/0040-1951(86)90006-5.

Biq, C. (1965), The East Taiwan Rift, *Petrol. Geol. Taiwan*, *4*, 93–106.

Bomford, G. (1980), *Geodesy*, 4th ed., 120 pp., Oxford Univ. Press, New York.

Chang, C. P., J. Angelier, C. Y. Huang, and C. S. Liu (2001), Structural evolution and significance of a mélange in a collision belt: The Lichi Mélange and the Taiwan arc-continent collision, *Geol. Mag.*, *138*, 633–651.

Chen, W. S., and Y. Wang (1986), Coastal range geology in eastern Taiwan (in Chinese with English abstract), report, Cent. Geol. Surv., Taipei.

Cheng, S. N., Y. T. Yeh, and M. S. Yu (1996), The 1951 Taitung earthquake in Taiwan, *J. Geol. Soc. China*, *39*, 267–285.

Ching, K.-E., R.-J. Rau, and Y. Zeng (2007), Coseismic source model of the 2003 Mw 6.8 Chengkung earthquake, Taiwan, determined from GPS measurements, *J. Geophys. Res.*, *112*, B06422, doi:10.1029/2006JB004439.

Gutenberg, B., and C. F. Richter (1954), *Seismicity of the Earth and Associated Phenomena*, 2nd ed., 310 pp., Princeton Univ. Press, Princeton, N. J.

Ho, C. S. (1988), *An Introduction to the Geology of Taiwan, Explanatory Text of the Geologic Map of Taiwan*, 2nd ed., 192 pp., Cent. Geol. Surv., Min. of Econ. Affairs, Taipei, Taiwan.

Hsu, T. L. (1956), Geology of the Coastal Range, eastern Taiwan, *Bull. Geol. Surv. Taiwan*, *8*, 39–63.

Hsu, T. L. (1962), Recent faulting in the Longitudinal Valley of eastern Taiwan, *Mem. Geol. Soc. China*, *1*, 95–102.

Hu, J. C., et al. (2007), Coseismic deformation revealed by inversion of strong motion and GPS data: The 2003 Chengkung earthquake in eastern Taiwan, *Geophys. J. Int.*, *169*, 667–674, doi:10.1111/j.1365-246x.2007.03359.x.

Kuochen, H., Y. M. Wu, C. H. Chang, J. C. Hu, and W. S. Chen (2004), Relocation of the eastern Taiwan earthquakes and its tectonic implications, *Terr. Atmos. Oceanic Sci.*, *15*, 647–666.

Lee, C., and S. B. Yu (1987), Horizontal crustal deformation in eastern Taiwan (in Chinese), paper presented at 6th Conference of Surveying and Its Application, Natl. Central Univ., Tainan, Taiwan.

Lee, W. H. K., F. T. Wu, and S. C. Wang (1978), A catalog of instrumentally determined earthquakes in China (magnitude76) compiled from various sources, *Bull. Seismol. Soc. Am.*, *68*, 383–398.

Liu, C. C., and S. B. Yu (1990), Vertical crustal movement in eastern Taiwan and its tectonic implications, *Tectonophysics*, *183*, 111–119, doi:10.1016/0040-1951(90)90191-A.

Maerten, F., P. Resor, D. Pollard, and L. Maerten (2005), Inverting for slip on three-dimensional fault surfaces using angular dislocations, *Bull. Seismol. Soc. Am.*, *95*, 1654–1665.

Malavieille, J., S. E. Lallemand, S. Dominguez, A. Deschamps, C.-Y. Lu, C.-S. Liu, P. Schnürle, and the ACT scientific crew (2002), Arc-continent collision in Taiwan: Marine observations and geodynamic model, *Spec. Pap. Geol. Soc. Am.*, *358*, 187–211.

Shyu, J. B. H., K. Sieh, Y. G. Chen, and C. S. Liu (2005), Neotectonic architecture of Taiwan and its implications for future large earthquakes, *J. Geophys. Res.*, *110*, B08402, doi:10.1029/2004JB003251.

Shyu, J. B. H., K. Sieh, Y. G. Chen, and L. H. Chung (2006), Geomorphic analysis of the Central Range fault, the second major active structure of the Longitudinal Valley suture, eastern Taiwan, *Geol. Soc. Am. Bull.*, *118*, 1447–1462, doi:10.1130/B25905.1.

Shyu, J. B. H., L. H. Chung, Y. G. Chen, J. C. Lee, and K. Sieh (2007), Re-evaluation of the surface ruptures of the November 1951 earthquake series in eastern Taiwan, and its neotectonic implications, *J. Asian Earth Sci.*, *31*, 317–331, doi:10.1016/j.jseaes.2006.07.018.

Taiwan Weather Bureau (1952), The 1951 earthquake report (in Chinese), report, 83 pp., Taiwan Weather Bur., Taipei.

Teng, L. S. (1990), Geotectonic evolution of late Cenozoic arc continent collision in Taiwan, *Tectonophysics*, *183*, 57–76, doi:10.1016/0040-1951(90)90188-E.

Thomas, A. L. (1993), POLY3D, A three-dimensional, polygonal element, displacement discontinuity boundary element computer program with applications to fractures, faults, and cavities in the Earth's crust, MS. thesis, 62 pp., Dep. of Geol., Stanford Univ., Stanford, Calif.

Wessel, P., and W. H. F. Smith (1995), New version of the generic mapping tools released, *Eos Trans. AGU*, *76*, 329.

Wu, Y., M. Y. G. Chen, C. H. Chang, L. H. Chung, and T. L. Teng (2006), Coseismic versus interseismic ground deformations, inversion and segmentation revealed by 2003 *Mw* 6.8 Chengkung earthquake in eastern Taiwan, *Geophys. Res. Lett.*, *33*, L02312, doi:10.1029/2005GL024711.

Yu, S. B. (1989), Crustal deformation in the Longitudinal valley area (in Chinese), Ph.D. thesis, 161 pp, Natl. Central Univ., Jhongli, Taiwan.

Yu, S. B., and L. C. Kuo (2001), Present-day crustal motion along the Longitudinal Valley Fault, eastern Taiwan, *Tectonophysics*, *333*, 199–217, doi:10.1016/S0040-1951(00)00275-4.

Yu, S. B., and C. C. Liu (1989), Fault creep on the central segment of the Longitudinal Valley fault, eastern Taiwan, *Proc. Geol. Soc. China*, *32*, 209–231.

Yu, S. B., D. D. Jackson, G. K. Yu, and C. C. Liu (1990), Dislocation model for crustal deformation in the Longitudinal Valley area, eastern Taiwan, *Tectonophysics*, *183*, 97–109, doi:10.1016/0040-1951(90)90190-J.

Yu, S. B., H. Y. Chen, and L. C. Kuo (1997), Velocity field of GPS stations in the Taiwan area, *Tectonophysics*, *274*, 41–59, doi:10.1016/S0040-1951(96)00297-1.

G.-T. Chen and Y.-H. Lee, Department of Earth and Environmental Sciences, National Chung-Cheng University, 168 University Road, Ming-Hsiung, Chia-Yi, Taiwan. (nscoe@mail.eq.ccu.edu.tw; seilee@eq.ccu.edu.tw)

K.-E. Ching and R.-J. Rau, Department of Earth Sciences, National Cheng-Kung University, Number 1, University Road, Tainan City 701, Taiwan. (kuenmiao@yahoo.com.tw; raurj@mail.ncku.edu.tw)